Journal of Alloys and Compounds 627 (2015) 136–145

Contents lists available at ScienceDirect

Journal of Alloys and Compounds

journal homepage: www.elsevier.com/locate/jalcom

Morphology of the asymmetric iron–silicon interfaces

L. Badía-Romano [a,b,*], J. Rubín [a,c], F. Bartolomé [a,b], C. Magén [b,d,e], J. Bartolomé [a,b], S.N. Varnakov [f,g], S.G. Ovchinnikov [f,g], J. Rubio-Zuazo [h,i], G.R. Castro [h,i]

[a] Instituto de Ciencia de Materiales de Aragón, CSIC-Universidad de Zaragoza, E-50009 Zaragoza, Spain
[b] Departamento de Física de la Materia Condensada, Universidad de Zaragoza, E-50009 Zaragoza, Spain
[c] Departamento de Ciencia de Materiales e Ingeniería Metalúrgica, Universidad de Zaragoza, E-50018 Zaragoza, Spain
[d] Laboratorio de Microscopías Avanzadas (LMA), Instituto de Nanociencia de Aragón (INA), Universidad de Zaragoza, E-50018 Zaragoza, Spain
[e] Fundación ARAID, E-50004 Zaragoza, Spain
[f] Kirensky Institute of Physics, Siberian Division, Russian Academy of Sciences, Akademgorodok, Krasnoyarsk 660036, Russia
[g] Siberian Aerospace University, pr. im. gazety "Krasnoyarskii rabochii" 31, Krasnoyarsk 660014, Russia
[h] SpLine Spanish CRG beamline at the ESRF, 6 Rue Jules Horowitz, 38043 Grenoble, France
[i] Instituto de Ciencia de Materiales de Madrid, CSIC, Sor Juana Inés de la Cruz, Madrid, Spain

ARTICLE INFO

Article history:
Received 24 October 2014
Received in revised form 4 December 2014
Accepted 5 December 2014
Available online 13 December 2014

Keywords:
Fe/Si nanolayers
Interfaces
Fe silicides
Compositional depth
HAXPES
CEMS

ABSTRACT

A systematic study of the iron–silicon interfaces formed upon preparation of (Fe/Si) multilayers has been performed by combination of modern and powerful techniques. Samples were prepared by thermal evaporation under ultrahigh vacuum onto a Si(100) substrate. The morphology of these films and their interfaces was studied by a combination of scanning transmission electron microscopy, X-ray reflectivity, angle resolved X-ray photoelectron spectroscopy and hard X-ray photoelectron spectroscopy. The Si-on-Fe interface thickness and roughness were determined to be 1.4(1) nm and 0.6(1) nm, respectively. Moreover, determination of the stable phases formed at both Fe-on-Si and Si-on-Fe interfaces was performed using conversion electron Mössbauer spectroscopy on multilayers with well separated Si-on-Fe and Fe-on-Si interfaces. It is shown that while a fraction of Fe remains as α-Fe, the rest has reacted with Si, forming the paramagnetic c-$Fe_{1-x}Si$ phase and a ferromagnetic Fe rich silicide (DO_3 type phase). We conclude that the paramagnetic c-$Fe_{1-x}Si$ silicide sublayer is identical in both Si-on-Fe and Fe-on-Si interfaces, whereas an asymmetry is revealed in the composition of the ferromagnetic silicide sublayer.

1. Introduction

A large amount of work has been dedicated to the growth and characterization of ferromagnetic metal/semiconductor nanostructures because of their unique physical properties for applications in Spintronics [1–8]. Particularly, a lot of this attention has been focused on the case of Fe/Si multilayer magnetic structures since they are quite compatible with Si microchip technology. However, in this type of multilayers, technical issues arise from the atomic diffusion and iron silicides formation at the Fe/Si interface during the deposition process. Indeed, iron silicides at the interfaces can affect their physical properties and possible applications [9,10]. Therefore, a characterization of the Fe–Si interfaces, including the morphology and formation of iron silicides during the deposition process, is of paramount importance.

The silicide formation at the Si-on-Fe and Fe-on-Si interfaces is known to be asymmetric [11,12,14,15]. In spite of the work done on this subject, there are contradictions in the literature; for example, the sequence of phase formation is still unclear. Different silicide phases like FeSi [16,17,14], c-$Fe_{1-x}Si$ [18,19,12], $FeSi_2$ [20,17,15] and Fe_3Si [11,21,22] have been proposed to be formed at the Fe-on-Si interface. In contrast, in the Si-on-Fe interface some authors report only the presence of the paramagnetic c-$Fe_{1-x}Si$ ($0 \leqslant x \leqslant 0.5$) [11,19,12,23], while others state that a ferromagnetic Fe rich Fe(Si) solid solution is also present [18,15,24]. The contradictions may be caused by differences in the samples used; specifically, the substrate and the number and thickness of the Si and Fe layers. It is unclear if some of the results can be assigned to single Si/Fe interfaces, or they should be ascribed to the interfaces in particular $(Fe/Si)_n$ systems.

To contribute to clarify this situation the present work deals with an exhaustive study on the morphology and composition of the Fe–Si interfaces as a function of depth. Firstly, we proceeded to study a Si-on-Fe interface on a single (Si/Fe) bilayer deposited

* Corresponding author at: Instituto de Ciencia de Materiales de Aragón, CSIC-Universidad de Zaragoza, E-50009 Zaragoza, Spain.
E-mail address: lbadia@unizar.es (L. Badía-Romano).

http://dx.doi.org/10.1016/j.jallcom.2014.12.019
0925-8388/

on a passivated Si substrate, by means of a combination of techniques. Specifically, we performed scanning transmission electron microscopy (STEM) imaging combined with electron energy loss spectroscopy (EELS) and X-ray reflectivity (XRR) for the morphological characterization, whereas for the compositional study, angle resolved X-ray photoelectron spectroscopy (ARXPS) combined with hard X-ray photoelectron spectroscopy (HAXPES) were used. Secondly, we aimed to elucidate the differences in silicide composition existing between the Fe-on-Si and Si-on-Fe interfaces. The information on the Fe–Si interface constituents was obtained by using the isotope selective technique, conversion electron Mössbauer spectroscopy (CEMS). To this end we prepared a series of samples consisting of a triple repetition of the (Si/Fe) stack deposited on a SiO_2 substrate, containing ^{57}Fe probe layers placed at different regions in the Fe layers, and Fe layer thickness large enough to ensure that the two Si/Fe interfaces could be observed separately.

All the studied samples were prepared by thermal evaporation in the molecular-beam epitaxy "Angara" set-up [25] under ultra-high vacuum. A Si(100) substrate prepared by Shiraki method was used [26]. The background pressure was better than 1.0×10^{-7} Pa. Elements were evaporated from boron nitride crucibles. Growth rates were 0.4 nm/min for ^{57}Fe, 2.5 nm/min for ^{56}Fe and 1.7 nm/min for Si, which was checked *in situ* by high speed laser ellipsometry. Final thickness was measured *ex situ* by X-ray fluorescence. All the Fe and Si layers were deposited at room temperature (RT). After fabrication, all the studied samples were exposed to air.

2. Morphological study of the Si-on-Fe interface

The morphological characterization of the Si-on-Fe interface was performed on a single (Si/Fe) bilayer grown on a Si(100) substrate with thickness sequence Si(100)/SiO_x/Fe(18 nm)/Si(4.3 nm).

2.1. Microstructure characterization

High angle annular dark field (HAADF) STEM imaging combined with EELS was performed on the (Si/Fe) bilayer in a probe corrected FEI Titan Transmission Electron Microscope equipped with a Gatan Tridiem 866 ERS energy filter and operated at 300 kV. To prepare the transversal section with FIB for (HAADF) STEM measurements a Pt layer is deposited as a step in the process of cutting. The HAADF-STEM image (Fig. 1) reveals a good layer by layer growth in spite of some appreciable roughness observed at the interfaces. The STEM-EELS profile shows the presence of a SiO_x passivating buffer layer on the Si substrate. This buffer layer has 20(4)% oxygen content and a maximum of 35(4)% on its surface. On top of it, the Fe layer is shown to be polycrystalline with no oxygen content. An Fe layer thickness of 20(3) nm is obtained from this profile, which compares well with the nominal value of 18 nm. The Si layer deposited on the Fe one is oxygen free until the naturally oxidized SiO_2 region by contact with air. Finally the auxiliary Pt thick overlayer is observed on top. The thicknesses of the pure Si and SiO_2 layers in the upper-most deposited layer are determined by XRR in the next section.

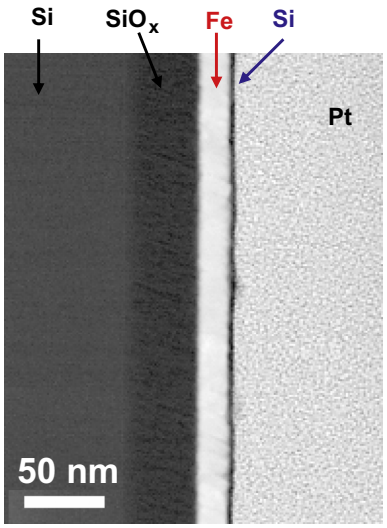

Fig. 1. HAADF-STEM image of the (Si/Fe) bilayer. A Pt layer was deposited on top of the sample for protection.

2.2. Reflectivity measurements

X-ray reflectivity (XRR) was measured on the (Si/Fe) bilayer to deepen in determining its morphology and composition. The XRR experiment was carried out at the Spanish CRG Spline beamline at the European Synchrotron Radiation facility (ESRF), using photons of a fixed wavelength $\lambda = 0.9538$ Å (13 keV). The use of high energy photon radiation allows to obtain information at larger depths than with a conventional X-ray source.

The morphology and composition of the stack can be obtained from the fit of the experimental XRR data to a layer sequence model. Specifically, the oscillations periodicity and the intensity decay in the XRR curve provide the layer thickness and roughness, respectively. The analytical software LEPTOS with a Nevot–Croce model and the Genetic Algorithm as fitting method, was used to perform the XRR fit.

The XRR experimental data and the corresponding fit (solid line) are displayed in Fig. 2. Besides the layers observed by STEM (Fig. 1), an additional layer is required to achieve acceptable fits: an iron silicide phase between the Si and Fe layers (see the stack model of Table 1). Thickness, roughness and mass density at each layer were refined, except the densities of the pure Si and Fe layers which were fixed. The fitted values of each layer forming the stack are shown in Table 1.

The XRR results reveal that the deposited Si upper layer of 4.3 nm nominal thickness is naturally oxidized ($\rho = 2.60(10)$ g/cm^3) to be compared to crystalline SiO_2 ($\rho_C = 2.65$ g/cm^3) [28], but a pure Si layer of 2.8(1) nm thickness still remains. The iron silicide layer at the Si-on-Fe interface shows a thickness of 1.4(1) nm and $\rho = 5.05(10)$ g/cm^3. This fitted density is similar to that of the stable stoichiometric ϵ-FeSi phase ($\rho = 5.19$ g/cm^3 [29]), but it also

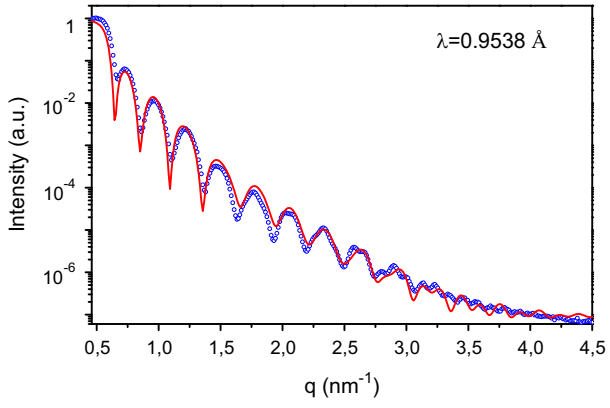

Fig. 2. XRR measurement on the Si/Fe bilayer. The experimental data are represented by the open circles while the solid line represents the corresponding fit [27]. Fitted thickness and roughness of each layer are summarized in Table 1.

Table 1
Fitted thickness, roughness and density values of each layer forming the Si/Fe bilayer, according to the stack model used in the XRR fit. The density values of the pure Si and Fe layers are both fixed parameters.

Stack model	Thickness (nm)	Roughness (nm)	Density (g/cm^3)
SiO_2	2.9(1)	1.3(1)	2.60(10)
Si	2.8(1)	0.8(1)	2.33
FeSi	1.4(1)	0.6(1)	5.05(10)
Fe	19.4(1)	0.8(1)	7.87
SiO_x	18.7(1)	0.7(1)	2.51(10)
Si substrate	–	–	2.33

lies between the value 4.73 g/cm^3 of the highly Fe-defective and epitaxially stabilized c-$Fe_{0.5}Si$ [30] and the close to stoichiometric c-$Fe_{0.88}Si$ [31], both with the CsCl structure. c-$Fe_{1-x}Si$ has been claimed to appear in the Fe/Si interface [18,19,12,15]. The fitted thickness has to be compared to a previous determination by GIXRR [14], where the Si-on-Fe interface showed also a thickness of 1.4 nm and the fitted optical constant turned out to be that of FeSi. Finally, a thickness of 19.4(1) nm is obtained for the Fe layer, which is in agreement with the value of about 20 nm from the STEM measurements. All the layers forming the stack, except the oxidized Si top layer, show roughness values lower than 1 nm, which indicates a good layer growth.

It is worth remarking that the interlayer region in the stacking sequence has been modelled differently in this work than in Refs. [13,14]. While we have used abrupt interfaces with a Nevot–Croce form, Refs. [13,14] used scattering length density (SLD) profile calculations, where each layer thickness was determined when the SLD attains that of the adjacent layer within a 10% difference. In either case silicides with Si content below 10% close to the α-Fe could have been neglected and therefore the obtained Si-on-Fe interface thickness [1.4(1) nm] should be considered as a lower limit.

2.3. X-ray photoelectron spectroscopies

In order to obtain information on the composition of buried layers and interfaces as a function of depth, we use two specific non-destructive XPS techniques. On one hand, angle-resolved X-ray photoelectron spectroscopy (ARXPS) provides depth profiling based on tilting the specimen with respect to the analyzer, to obtain XPS spectra at several angles of emission [32]. On the other hand, hard X-ray photoelectron spectroscopy (HAXPES), which consists of XPS performed with high energy photons and fixed geometry; working with high variable photon energy and subsequent kinetic energy of the produced photoelectrons allows to probe interfaces and layers that are buried at sample positions ten times deeper than in a standard XPS.

In this section, the experimental data are shown in terms of the binding energy (E_{BE}), $E_{BE} = E_{ph} - E_{Kin}$, where E_{ph} is the photon energy and E_{Kin} the kinetic energy of the photoelectrons.

2.3.1. Angle resolved X-ray photoelectron spectroscopy (ARXPS)

ARXPS measurements at the Si 2p and Fe 2p core-levels were performed on the Si/Fe bilayer, at RT and fixed photon energy. The spectra were collected using a hemispherical analyser (SPECS EA-10 Plus). A twin anode (Mg and Al) X-ray source was operated at a constant power of 120 W; the Al Kα radiation was chosen ($E_{ph} = 1486.7$ eV). Spectra at emission angle, ψ, from 0° to 75° in steps of 15° were acquired sequentially by tilting the sample with respect to the analyser. The emission angle is referred to the surface normal, so that photoelectrons emitted perpendicular to the surface emerge at $\psi = 0°$. As the emission angle changes, the depth from which information can be obtained varies, which is the key-feature of ARXPS.

The Si 2p and Fe 2p core-level spectra taken at increasing emission angles $\psi = 0°$, 30° and 75°, are displayed in Fig. 3(a) and (b), respectively. The fits of the spectra were performed with CasaXPS sofware, using a Shirley type background and Voigt peak lineshape. It should be recalled that the spectrum at a given emission angle, i.e., a given information depth (Σ), includes the information of spectra of larger emission angles (shorter Σ).

The 84–108 eV region shows the Si 2p and Fe 3s core-level spectra at all emission angles, except for $\psi = 75°$, where only the Si 2p spectrum is observed. The fit of the Si 2p core-level part required five peaks at binding energies of 99.3, 99.8, 100.8, 102.4 and 103.1 eV (values for $\psi = 0°$) (see Fig. 4(b)). The peaks at 103.1, 102.4 and 100.8 eV are shifted by 3.8, 2.1 and 1.0 eV with respect to the 99.3 eV Si^0 $2p_{3/2}$, so the peak at 103.1 eV will be assigned to Si^{+4} (SiO_2) and the other two to SiO_x suboxides [33]. The peak at 99.8, i.e., shifted by +0.6 eV with respect to Si^0 $2p_{3/2}$ originates either by Si in an iron silicide [34] or the Si^0 $2p_{1/2}$ component [35,36]. While the ratio of intensities of the Si^0 $2p_{1/2}$ and Si^0 $2p_{3/2}$ doublet is 1/2 for a single Si phase, an additional contribution of Si from an Fe silicide should increase the observed ratio. Fig. 4(a) shows this ratio as a function of the emission angle, where a clear increase is observed for angles below 50°, i.e., for increasing probed depth, which shows the presence of the Fe silicide.

The estimation of the depth at which the Fe silicides appear using ARXPS data requires to relate the emission angle and the information depth Σ, i.e., $\Sigma = -\lambda_{in} \cos\psi \ln[(1/(1 - P/100)]$, where P is the percentage of photoelectrons by the time they reach the surface and λ_{in} is the inelastic mean free path (IMFP) [37]. The usual $P = 95\%$ was chosen, whence $\Sigma = 3\lambda_{in}cos\psi$. However, elastic scattering effects can be important and dependent on the emission angle [37]. The practical information depth, S, which includes the elastic scattering effects can be calculated as $S = R\Sigma$, with $R = 1 - 0.787\omega$ for $0 \leqslant \psi \leqslant 50°$ and the single-scattering albedo $\omega = \lambda_{in}/(\lambda_{in} + \lambda_t)$ [37]. λ_t is the transport mean free path (TMFP) [37,38].

In order to estimate the information depth at the present measurements, the studied multilayer will be simplified to a single layer of Si on a flat Fe substrate. IMFP values were obtained from the NIST database SDR 71 [39] and TMPF values through the NIST Elastic-Scattering Cross-Section Database SDR 64 [40], for the photoelectron kinetic energies in the Si 2p region. At $\psi = 0°$, practical information depth values, $S = 8.7$ and 5.3 nm for the Si 2p and Fe 2p regions, respectively, were obtained. This accounts for 95% of the photoelectrons produced at Si or Fe atoms and passing through a single Si overlayer. If the Si layer is substituted by a SiO_2 layer, similar S values are obtained, $S = 10.8$ and 6.3 nm for the Si 2p and Fe 2p regions, respectively, so that the actual structure of the deposited Si top layer should not affect the information from the deeper Fe and Fe silicide layers. For $\psi = 50°$ where Fe silicides start to show up, $S = 5.6$ nm was obtained, which is consistent with the XRR determination of a SiO_2 + Si top layer thickness of 5.7 nm.

The Fe 2p core-level spectra (Fig. 3(b)) were well fitted with four components. The peaks at $E_{BE} = 706.8$ eV and 719.8 eV, correspond to the Fe^0 $2p_{3/2}$ and Fe^0 $2p_{1/2}$ levels, respectively, and they were fitted with the 2:1 relationship in the areas. They may correspond to pure Fe or Fe in a Fe-rich alloy in the buried Fe layer. The peak at $E_{BE} = 707.13$ eV, i.e. shifted +0.3 eV with respect to the Fe^0 $2p_{3/2}$ peak, is assigned to the FeSi phase [41,34,42,13,43–47]. Finally, the peak at $E_{BE} = 711.6$ eV has been previously assigned to a plasmon of Fe silicides [45,48]. The alternative interpretation of this peak as an Fe oxide can be discarded by the EELS analysis in Section 2.1 above.

2.3.2. Hard X-ray photoelectron spectroscopy (HAXPES)

The Si 1s and Fe 1s core-level HAXPES spectra were collected at the SpLine beamline of the ESRF. The photoemission peaks were

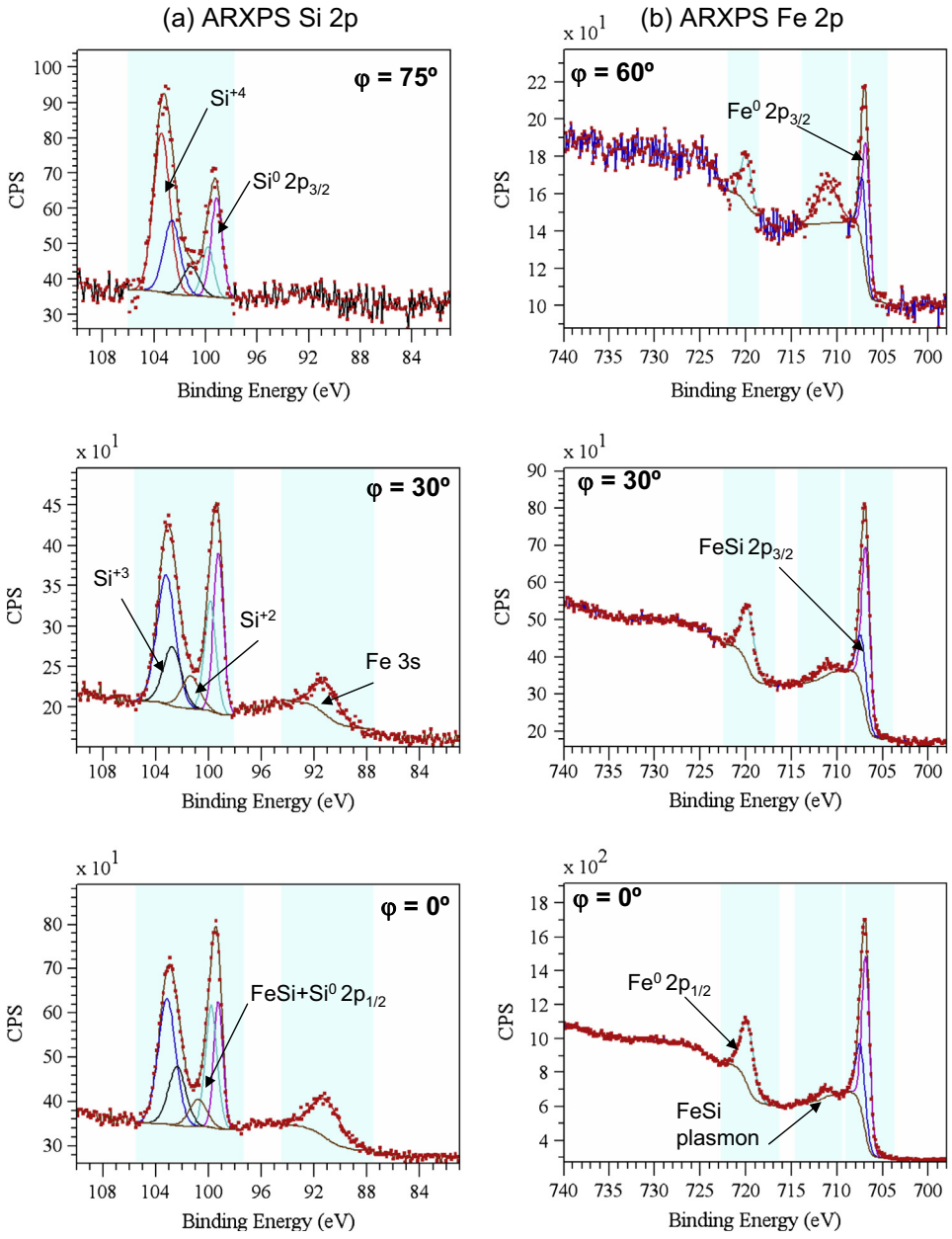

Fig. 3. (a) ARXPS Si 2p spectra and (b) ARXPS Fe 2p spectra at different emission angle values.

measured for increasing incident photon energies (E_{ph}); therefore increasing photoelectron kinetic energies were involved (E_{Kin}) and information depths larger than in conventional soft X-rays XPS were accessible. The spectra were corrected for the photon flux, the detector efficiency, the analyser transmission function and the photoionization cross sections of the Fe 1s and Si 1s subshells [49–51]. The normalized HAXPES spectra as a function of E_{ph} (from 9 to 15 keV) are shown in Fig. 5.

In a similar way to XPS above, the practical information depth can be estimated. Because of the much higher kinetic energies of photoelectrons, larger S values are expected, and both Si 1s and Fe 1s spectra will include electrons which have traveled through the ≈18 nm-thick Fe layer and the SiO_2/Si capping layer. Since NIST databases can provide the IMFP in a limited kinetic energy range, they are only useful for the lowest photon energies. Therefore, in the case of HAXPES we will make use of IMFP and single scattering albedo from Ref. [52]. Neglecting the capping Si layer, i.e., assuming that electrons will only travel through Fe, S for the Si 1s spectra from 22 nm to 39 nm for E_{ph} = 9 to 15 keV can be estimated. Since albedo for Si is smaller than for Fe [52], including the capping layer will only produce larger S values. Such large values of the practical information depth in the Si 1s spectra suggest that the oxidized Si substrate could show up in the spectra.

Both Si and Fe HAXPES spectra show a very important background below the intrinsic 1s core level peaks, which increases with increasing incident photon energy. In order to obtain binding energies of the involved core level through a fit of the measured spectra with peak lineshapes, the background has to be included. The complexity of the 1s spectra, even in single element samples, requires the use of a Tougaard background to account for extrinsic energy loss processes and the modelling of the contribution of the intrinsic energy loss processes [53,54]. The application of such complex procedure to the present samples, where several compounds contribute to the spectra, is out of the scope of the present work. For practical purposes, a Tougaard background was used, and the intrinsic energy loss processes were simulated by a broad

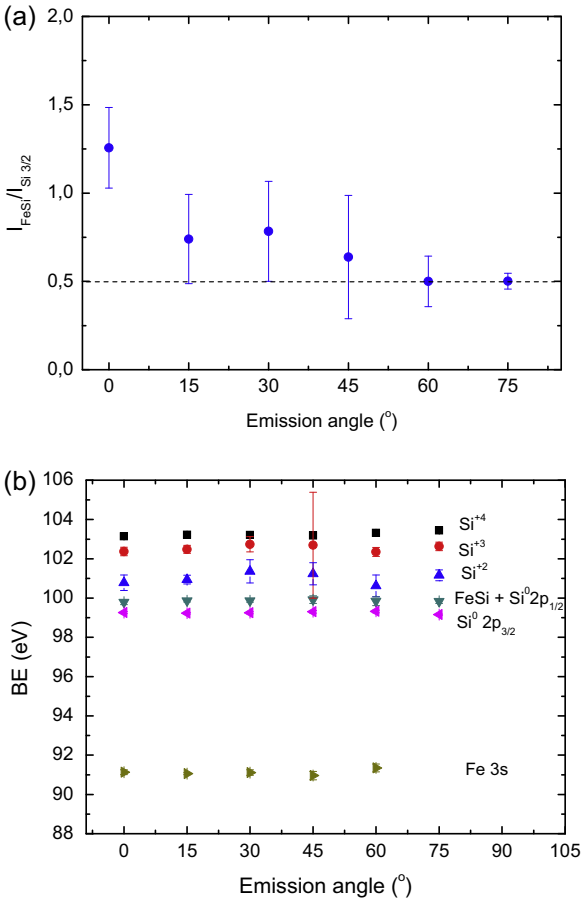

Fig. 4. (a) Ratio of the intensities of the FeSi + Si^0 $2p_{1/2}$ and the Si^0 $2p_{3/2}$ peaks, as a function of the emission angle. (b) Peak positions (BE) of the indicated peaks as a function of the emission angle.

lineshape centered at the bulk plasmons and additional lineshapes between the plasmon and the highest contribution in the spectra produced by the core level photoelectrons. This allows to obtain a set of binding energies from the data, which will be discussed below.

2.3.2.1. Si 1s spectra. Fig. 5(a) shows the spectra of the Si 1s core level. These are dominated by two main features, which have been fitted with three components: a peak at $E_{BE} = 1838.9$ eV, corresponding to the Si^0 1s core-level [55–59] and two peaks with binding energies shifted ∼+3.3 and +4.5 eV with respect to Si^0, one of which should be assigned to SiO_2 at the outermost layer [55–57], as in the ARXPS spectra. Since the Si 1s peak from SiO_2 should appear at a binding energy shift +0.62 eV higher than in Si 2p [60], the peak with the chemical shift of +4.5 eV will be assigned to SiO_2.

The present HAXPES experiment does not allow to resolve a core-level peak to be assigned to an Fe silicide in the same way as we found by ARXPS at a binding energy shift of +0.6 eV with respect to the main Si^0 peak. Indeed, the total instrumental resolution, which includes the analyser resolution and the photon line energy width, ranged between 2.0 and 2.7 eV, depending on E_{ph}. However, the iron silicide could show up in a different way. In fact, the low binding energy "pre-peak" in the Si spectra, shifted ≈−3.5 eV with respect to Si^0 1s, is also found in the Fe spectra with a shift of ≈−5 eV with respect to Fe^0 1s (Fig. 5), which suggests that it is produced by an Fe silicide compound. Such "pre-peaks" have been observed in XPS Fe 2p spectra of Fe oxides [61] with a binding energy shift of ≈−2 eV and were attributed to defects at the sample surface produced by the mechanical preparation process giving rise to iron suboxides. In the case of the buried $Fe_{0.5}Si$ phase formed at the Si/Fe interface, this is an iron defective and strained phase [12] with a very small thickness of approximately 0.5 nm [12]. Then, this silicide layer has a large surface to volume ratio, where Si and Fe atoms in the iron silicide can contribute to a spectrum in two forms; as bulk, and as strained surface, so that an additional low intensity "pre-peak" of defects origin could appear. We note that, in contrast to HAXPES, where large IMPSs are involved, the "pre-peaks" are not observed in the Si 2p and Fe 2p ARXPS spectra because of the much shorter IMFP and consequent smaller contribution of the iron silicide to the total spectral intensity.

2.3.2.2. Fe 1s spectra. It is the first time that the Fe 1s photoemission spectra of a multilayered system composed by not only metallic iron, but also other silicide phases, have been recorded as a function of the E_{ph}. In the analysis of the Fe 1s core level spectra (Fig. 5(b)), it is not trivial to separate all the different components which are overlaid [54]. As HAXPES allows to probe deeper than standard XPS, the main peak will contain not only the intrinsic bulk and surface contributions from the different Fe silicides at the interface layer, but also those from the metallic Fe present in the buried Fe layer. Additionally plasmons appear in the high binding energy region. Here, we will present a qualitative description of the data.

Fig. 5(b, upper panel) shows the Fe 1s spectra measured at different E_{ph} energies. As a representative example, we discuss here the Fe 1s spectrum measured at $E_{ph} = 9$ keV, which is shown in Fig. 5(b, middle panel). The bulk plasmon loss for Fe 1s [54] is observed as a very broad peak centred at $E_{BE} = 7135$ eV. A "pre-peak" was also included in the fit to account for the tail at the low binding energy region. The peak at $E_{BE} = 7113$ eV corresponds to bulk metallic Fe (Fe^0) [54], while the peak shifted ∼+1.2 eV from the Fe^0 main peak comes from Fe silicide phases. Finally, the components with E_{BE} shifts ⩾+5 eV from the main peak can be related to surface intrinsic energy loss portions of Fe [54] and the Fe silicides.

The results of the photon spectroscopies have enabled to characterize the morphology and compositional depth profile of the (Si/Fe) bilayer. Specifically, the STEM-EELS measurements have shown the existence of some oxygen content in the first deposited Si layer (SiO_x layer) and an oxidized Si layer in the sample surface. Additionally the XRR results along with ARXPS and HAXPES also showed SiO_x suboxides at the surface layer, and the presence of a Si-on-Fe interface with a thickness of 1.4(1) nm and a roughness of 0.6(1) nm at a depth of ≈ 5.7 nm, mainly consisting of the c-$Fe_{1-x}Si$ phase. This information about the (Si/Fe) bilayer has been summarized in a schematic image of the multilayer stack (see Fig. 6).

We note that the thickness and roughness values of the Si-on-Fe interface obtained from XRR and those reported previously for Fe/Si multilayers fabricated with e-beam deposition [13] and ion-beam deposition [15] on different substrates are in excellent agreement.

3. Compositional study of the Si-on-Fe and Fe-on-Si interfaces by CEMS

The study of the Fe/Si interfaces by means of CEMS has been previously attempted by Strijkers et al. [12], Gupta et al. [15] and Badía-Romano et al. [27,24]. The selectiveness of ^{57}Fe to probe specific regions in a multilayered structure by the deposition of thin layers of ^{57}Fe into a ^{56}Fe layer (the use of ^{56}Fe guarantees that the CEMS signal only comes from the ^{57}Fe probe layer) can be a

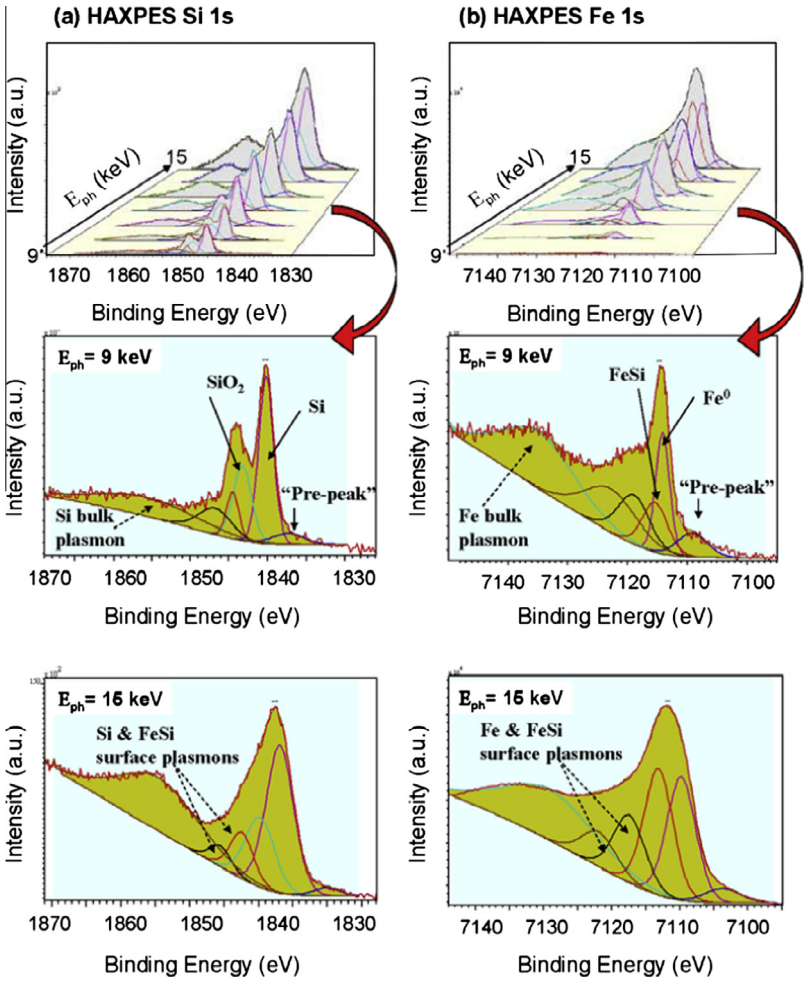

Fig. 5. (a) HAXPES Si 1s spectra, (b) HAXPES Fe 1s spectra, (measured at RT). (Upper panels) HAXPES spectra at different E_{ph}, (middle and lower panels) HAXPES spectra at the lowest and highest E_{ph}, E_{ph} = 9 and 15 keV, respectively.

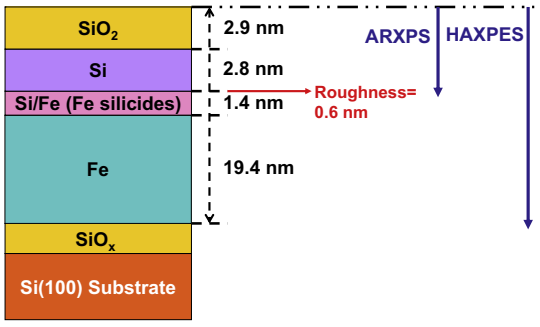

Fig. 6. Schematic image of the as-deposited (Si/Fe) bilayer. Blue arrows indicate the maximum information depth that can be obtained by the different techniques, STEM, XRR, ARXPS and HAXPES. (For interpretation of the references to color in this figure legend, the reader is referred to the web version of this article.)

very powerful tool. Especially, an asymmetry between the Si-on-Fe and Fe-on-Si interfaces has been proposed, which has also been derived from other type of experiments [14]. Notwithstanding, before new CEMS spectra are presented and analyzed, it is relevant to make a few comments with respect to the use of the thin ^{57}Fe probe layers method:

(1) It has been proved that the Fe/Si interface contains a paramagnetic silicide, claimed to be the epitaxially stabilized c-$Fe_{1-x}Si$ paramagnetic phase with a thickness of about 0.4–0.5 nm [19,12,23]. Additionally, a ferromagnetic $Fe_{1-x}Si_x$ phase has also been observed with an estimated Si atomic concentration in the range 15–18% [12,24]. However, since in all multilayers studied by CEMS the Fe layers had a thickness from 3.1 to 4 nm, it is unclear whether the $Fe_{1-x}Si_x$ phase with the proposed concentration is intrinsic to a single Fe/Si interface or it is the average concentration produced by interdiffusion from the two Si spacers into the sandwiched Fe layer. On one hand, no sextet with hyperfine values of α-Fe were detected at the centre of the Fe layers, which would have marked the separation of the two Si/Fe interfaces. On the other hand, from reflectivity measurements [13,14] on bilayers and multilayers the total Si-on-Fe plus Fe-on-Si interface thickness was determined to be about 2 nm. Consequently, the ^{57}Fe layers (0.6 nm [12] or 2 nm [15]) might not give intrinsic information of a single Si/Fe interface as long as the ferromagnetic phase is concerned, but instead information of the Si/Fe interfaces in the particular fabricated multilayers. In order to discriminate between the Si-on-Fe and Fe-on-Si interfaces, the Fe layer thickness has to be large enough to contain an unambiguous α-Fe region at the centre separating both interfaces.

(2) The deposition of an ^{57}Fe layer introduces a new stage in the fabrication process. When it is deposited directly onto a Si layer it reacts with it and silicides are produced. In contrast, when it is deposited onto a ^{56}Fe layer just before the subsequent Si layer is added, intermixing of the two nuclear species can take place,

a ^{57}Fe/^{56}Fe interface is formed with non-zero roughness and therefore the nominal 0.6 nm ^{57}Fe layer could probe a larger region than expected.

(3) The characteristics of the CEMS measurement technique can also make difficult the analysis of the Si/Fe interfaces in a multilayer system. When a repetition of the Si and Fe layers is used to improve the CEMS signal, it must be taken into account that the electron yield from layers at different depths is affected by electron absorption processes dependent on the depth. This is not an issue as long as the contribution from every ^{57}Fe layer is identical, but can make the quantitative analysis very complex if the silicide layer composition is different in any of the Fe layers.

The present CEMS measurements were performed on separately grown samples with 0.6 nm ^{57}Fe probe layers at the bottom, on top and at the middle of ^{56}Fe layers. In order to improve the CEMS signal, the samples were multilayers consisting of the triple repetition of the (Si/Fe) bilayer, where the ^{57}Fe probe layer was deposited on every Fe layer. Samples were grown on a Si(1 0 0) substrate plus a SiO_2 buffer by the same deposition method as explained above for the sample studied by HAXPES, with Fe layer thickness of 10 nm, where the 0.6 nm ^{57}Fe probe layer was included, and 6 nm of Si spacer. The sample Si(1 0 0)/SiO_2/[^{56}Fe(9.4 nm)/^{57}Fe(0.6 nm)/Si(6 nm)] × 3, is denoted below as S-u, and was intended to probe the Si-on-Fe interface, while the sample Si(100)/SiO_2/[^{57}Fe(0.6 nm)/^{56}Fe(9.4 nm)/Si(6 nm)] × 3, denoted S-b, was intended to study the Fe-on-Si (see Fig. 7, insets). To ensure that the three Fe-on-Si interfaces are identical, an additional sample, S*-b, was fabricated, where a Si layer was first deposited on the SiO_2 buffer, on which the ^{57}Fe layer was subsequently grown. Finally, sample S-m, with the ^{57}Fe layer in the middle of the Fe layers was used as reference of the separation of the silicide formation from the two limiting Si spacers.

The CEMS spectra were acquired at RT using a constant acceleration spectrometer with symmetrical waveform and a ^{57}Co (25 mCi) source. A Rikon-5 detector with a 96%He–4%N_2 mixture was used. The spectra were fitted with NORMOS program [62].

The spectra of the four produced samples are collected in Fig. 7. The reference sample, S-m, with the ^{57}Fe probe layer placed in the middle of the Fe layer, shows only one sextet with the hyperfine parameters of α-Fe and intensity ratios 3:4:1:1:4:3 (Table 2), i.e., with the magnetization parallel to the layer plane. No silicides are present at the centre of the 10 nm Fe layer.

The S-b sample shows a CEMS spectrum whose shape is clearly different from that of the S-u and S*-b samples. The main difference resides in its doublet intensity, which is about one half of the doublet intensity shown by the S-u and S*-b spectra. The qualitative and quantitative differences between the S-b and S*-b spectra come from the samples morphology. Indeed, S-b has only two real Fe-on-Si interfaces, since the third ^{57}Fe layer is deposited on the SiO_2 buffer. This proves the necessity of the S*-b sample, which has three identical Fe-on-Si interfaces.

The S-u and S*-b samples are expected to show the Si-on-Fe and Fe-on-Si interfaces, respectively, from the CEMS electron yield of the three presumably identical interfaces. The spectra contain a central paramagnetic intensity and a distribution of intensity that extends between prominent peaks compatible with an α-Fe-type sextet and the paramagnetic contribution (see Fig. 7). The spectra were fitted in two ways: (i) a doublet and a distributions of sextets with increasing hyperfine fields from 15 to 34 T at constant steps and linearly increasing isomer shifts, as in previous works [12,9,15,24] and (ii) a doublet and a reduced number of fully adjustable sextets to account for the remaining intensity. Method (ii) is intended to analyze the different types of Fe environments

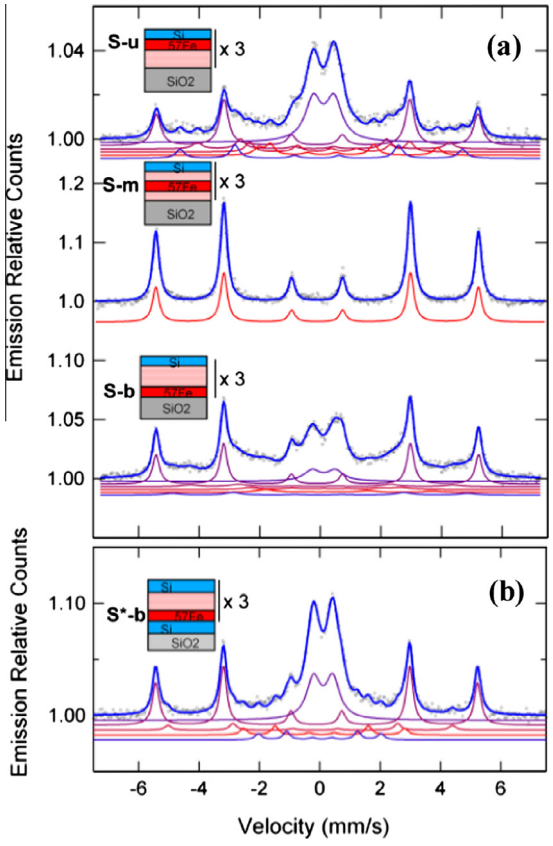

Fig. 7. (a) CEMS spectra of Si(1 0 0)/SiO_2/[Fe(10 nm)/Si(6 nm)] × 3 samples with a 0.6 nm ^{57}Fe probe layer deposited at various positions in the multilayer stack. (b) CEMS spectrum of the S*-b as-deposited sample.

and to try to get relevant information about the magnetic silicides in the interfaces. Up to five sextets were necessary to account for the intensity distribution in the spectra (Table 2).

The fitted doublets account for 50% of the total intensity in both spectra (S-u and S*-b), and they also show the same quadrupolar splitting $QS \simeq 0.67$ mm/s and isomer shift $\delta = 0.22$ mm/s, within experimental errors (Table 2). We conclude that the formation of the paramagnetic phase is symmetric at the Si-on-Fe and Fe-on-Si interfaces. This doublet is assigned to the paramagnetic c-$Fe_{1-x}Si$ phase [19,63,12,23]. This assignment does not rely on a well defined value of *QS*; in fact, stoichiometric c-FeSi with the ideal CsCl structure should show no quadrupole splitting, since it is cubic. However, values of *QS* from 0.43 mm/s to 0.68 mm/s in Si/Fe multilayers have been reported [18,12,15] and even a value of 0.8 mm/s in a single Fe/Si interface of Fe deposited onto a (7 × 7) reconstructed Si(1 1 1) surface has been found [19]. Since the *QS* splitting is caused by non-stoichiometric c-$Fe_{1-x}Si$ or interface stress which produce local non-cubic environments, its value can be very much dependent on the substrate and deposition method. Using the c-FeSi cell parameter $a = 0.55$ nm [30], the 50% of the nominal deposited ^{57}Fe thickness would result in an estimated thickness of the c-$Fe_{1-x}Si$ layer of 0.50(2) nm, which agrees with the values that can be estimated from Refs. [63–65,24].

The analysis of the sextets in terms of environments of Fe atoms has to take into account surface effects, since the ^{57}Fe probe layer is very thin and therefore a significant proportion of these atoms have local environments largely influenced by adjacent phases. Although a direct analysis in terms of a homogeneous phase as in bulk silicides is not possible, there is significant information that can be drawn from the spectra of samples S-u and S*-b:

Table 2
Fitting parameters of the as-deposited samples CEMS spectra. *I* refers to the relative intensity of each component with respect to the total area of the spectrum, and I_s indicates the relative intensity with respect to the sum of sextet areas. Isomer shifts are given with respect to α-Fe.

	S-u			
	QS (mm/s)	δ (mm/s)	*I*	
Doublet	0.68(1)	0.22(1)	0.49(1)	
	B_{hf} (T)	δ (mm/s)	*I*	I_s
Sextet #1	32.90(3)	0.004(4)	0.30(1)	0.59(2)
Sextet #2	28.9(1)	0.07(1)	0.009(6)	0.02(1)
Sextet #3	25.8(2)	0.05(2)	0.065(6)	0.13(1)
Sextet #4	18.3(2)	0.59(2)	0.071(5)	0.14(1)
Sextet #5	16.4(2)	0.65(2)	0.068(7)	0.13(1)
	S-m			
	B_{hf} (T)	δ (mm/s)	*I*	I_s
Sextet	33.02(1)	0.008(1)	1	1
	S-b			
	QS (mm/s)	δ (mm/s)	*I*	
Doublet	0.76(1)	0.23(1)	0.24(1)	
	B_{hf} (T)	δ (mm/s)	*I*	I_s
Sextet #1	33.02(2)	0.008(2)	0.32(1)	0.42(3)
Sextet #2	30.2(3)	0.08(2)	0.13(2)	0.17(2)
Sextet #3	26.9(3)	0.04(2)	0.13(2)	0.17(2)
Sextet #4	17.5(3)	0.51(3)	0.09(1)	0.12(1)
Sextet #5	15.4(5)	0.44(4)	0.10(1)	0.13(2)
	S-b*			
	QS (mm/s)	δ (mm/s)	*I*	
Doublet	0.65(1)	0.22(3)	0.51(1)	
	B_{hf} (T)	δ (mm/s)	*I*	I_s
Sextet #1	33.06(1)	0.007(2)	0.34(1)	0.70(2)
Sextet #2	28.3(1)	0.01(2)	0.034(4)	0.07(1)
Sextet #3	21.0(2)	0.34(2)	0.028(4)	0.06(1)
Sextet #4	17.5(1)	0.68(2)	0.044(4)	0.09(1)
Sextet #5	16.1(1)	0.07(2)	0.042(4)	0.09(1)

(i) As long as the recoilless fraction is assumed to be the same for any Fe environment, the sextets intensities are proportional to the Fe site environment probabilities, while the hyperfine field values are determined by the number of Fe nearest neighbors (n.n.). In bulk silicides, a $B_{hf} \simeq 33$ T sextet with high intensity is indicative of low Si concentration $Fe_{1-x}Si_x$ alloys ($x < 0.1$), where the Fe environment with 8 Fe n.n. has the highest probability, while a sextet with $B_{hf} < 19$ T appears only at concentrations higher than $x = 0.25$ [66,67], where environments with 3 Fe n.n. become significantly probable. The presence of both types of sextets in the present spectra reveals an apparent contradiction that may happen if results from bulk samples environments are used in such a thin ^{57}Fe layer. In fact, since 50% out of the 0.6 nm of the ^{57}Fe probe is in the paramagnetic silicide, only about 0.3 nm (or < 3 ML) of the nominal deposited probe layer is available to disclose other silicides at the Fe/Si interface and is therefore highly influenced by the close paramagnetic silicide phase. In the present case, the sextets with the lowest hyperfine fields (sextet #5 of S-u and S*-b in Table 2) can be assigned to Fe atoms close to the c-FeSi layer, where environments with few Fe atoms are most likely.

(ii) The intensity distribution among the sextets is different in each spectrum, which shows that there is an asymmetry in the Fe/Si interfaces, and it resides in the ferromagnetic silicides and not in the paramagnetic phase. The spectra are dominated by a ≈ 33 T sextet, which should correspond to Fe nuclei with the highest number of Fe n.n., either in a very low Si-content silicide, or α-Fe. Since the on top and at the bottom ^{57}Fe layers have the same nominal thickness, and the contribution to the spectra of the paramagnetic silicide phase is identical, the higher probability of the ≈ 33 T sextet in the Fe-on-Si interface indicates that the thickness of the remaining ferromagnetic $Fe_{1-x}Si_x$ alloy is narrower than the Si-on-Fe one, as proposed by Naik et al. [14].

The assignment of individual sextets to specific Fe environments in very thin layers should take into account the effect of second and third n.n. on the hyperfine field values, since some such neighbors could be missing at the interfaces and Fe atoms at those positions can constitute an important part of the total contribution to the CEMS spectra because of the large surface to volume ratio. In fact, in bulk magnetic silicides second and third n.n. contribute to a decrease in B_{hf} by as much as ≈ 0.73 T *per* Si atom [68,69]. Therefore, the fitted values of B_{hf} in the present spectra could be lower than those in bulk silicides with the same first n.n. environment, in particular for Fe atoms close to the c-$Fe_{1-x}Si$ paramagnetic phase. Then, the sextets in the sample S-u spectrum, which includes the low intensity sextet #2 (Table 2), are compatible with environments similar to those in a bulk $Fe_{1-x}Si_x$ silicide with x in the range 0.18–0.20 [66]. In contrast, the spectrum of samples S*-b, where that sextet #2 contributes to the spectrum as much as the others, would require first n.n. environments similar to those in the silicides with $x \leqslant 18$.

The spectral analysis method used in this work leads to different conclusions than those from the sextet distribution analysis method applied by other authors. The latter method can overestimate the sextet contribution to the spectrum in detriment of that of the paramagnetic doublet, as the separation between both spectral components will depend on the lower limit of the hyperfine field range and the actual composition of the magnetic silicide phases at each interface. In fact, the fit of the present spectra with a distribution of sextets with hyperfine field ranging from 15 to 34 T produces a doublet area of 46.5% and 30.5% for the Si-on-Fe and Fe-on-Si interfaces, respectively, i. e., lower values than with the individual sextet method, and an asymmetry is also obtained. This has to be compared to the doublet areas found in previous works on multilayers, analyzed with the sextet distribution method. In 4 nm thick Fe layer samples and sextet distribution with lower limit of 10 T [15], the respective doublet areas found were 18% and 26% of the deposited ^{57}Fe layer, while in 3.1 nm thick Fe layer samples [12] those areas were 29% and 15%, the opposite to Ref. [15], and much larger doublet intensity percentage per nm of deposited ^{57}Fe. Moreover, on similar multilayers with only 2.6 nm thick Fe layers with a particular ^{57}Fe probe layer deposition sequence, the analysis of CEMS spectra with the individual sextet method yielded to doublet areas of 16% in both interfaces [24], i.e., symmetric with respect to the paramagnetic sublayer, but of the order of those obtained in previous works [12,15], where a distribution of sextets were used. Thus, we note that (a) the asymmetry in the paramagnetic phase appears in Refs. [12] and [15] as a result of the sextet distribution analysis and (b) that for Fe thickness below 4 nm there is no clear separation of the two Fe/Si interfaces.

Recently the interface structure and composition of similar Fe/Si multilayer structures have been studied by X-ray magnetic circular dichroism (XMCD) in the electron yield mode [22]. Using the surface sensitivity of XMCD, the authors have related the exponential decrease for increasing depth of the emitted photoelectron yield to a model of interface with a nonmagnetic FeSi layer and a magnetic layer with a linear spatial distribution of $Fe_{1-x}Si_x$ solid solution from Fe_3Si to α-Fe. For a sample with the layer sequence $Si(100)/SiO_2/(Fe/Si)_3$ with Fe thickness of ~10 nm and Si thickness of 1.1 nm, and with the restriction of a full Fe/Si interface thickness as determined by XRR [14], a nonmagnetic FeSi thickness of

0.23 nm and a magnetic solid solution layer thickness of 1.17 nm for the Si-on-Fe interface were found. Besides, for the Fe-on-Si interface, a sample with Fe thickness ~8 nm and Si thickness of 1.5 nm was used. At this interface, the thicknesses of the nonmagnetic and magnetic parts were determined to be 0.15 and 0.55 nm, respectively [22]. The values of the nonmagnetic phase thickness in Ref. [22] are smaller than the estimation of 0.50(2) nm in this work and those obtained from Refs. [63–65,24], which range from 0.32 to 0.55 nm per interface. In those works multilayers with smaller Fe layer thickness than in the present paper were used.

As commented above in the section on the XRR results, the XRR determination of the thickness of the total Fe/Si interface could be underestimated, since it neglects low concentrations of the $Fe_{1-x}Si_x$ solid solution. However, the model used in Ref. [22] included a linear spatial distribution of $Fe_{1-x}Si_x$ solid solution from Fe_3Si to α-Fe, in the thickness determined by XRR (1.4 nm for the Si-on-Fe interface). If in the model of [22], the total Si/Fe interface thickness, without neglecting low concentration solid solutions, were larger than considered, then the resulting nonmagnetic phase thickness would result in a larger value, thus approaching the results shown in previous [63–65,24] and in the present work. As for the asymmetry in the nonmagnetic part found in that XMCD work, contrary to our conclusion of symmetric contributions derived from the CEMS analysis, it also depends on the mentioned hypothesis restricting the total interface thickness, on one hand, but it could be an effect of using such a thin Si layer deposited thickness in the XMCD measured samples, on the other.

4. Conclusions

We performed an exhaustive study of the iron silicide formation at the interfaces of as-deposited (Fe/Si) multilayered structures. Firstly, the morphology and compositional depth profile of a (Si/Fe) bilayer was determined by combination of STEM, XRR, ARXPS and HAXPES. A thickness value of 1.4(1) nm and a roughness of 0.6(1) nm were found for the studied Si-on-Fe interface, in agreement with previous results [13,15].

Additionally, the stable phases formed at both types of interfaces (Fe-on-Si and Si-on-Fe) on specific $(Fe/Si)_3$ multilayered samples was determined by CEMS. This powerful technique has allowed us to identify and quantify the different silicide phases which compound the probed zone of each interface.

In contrast to previous CEMS data on Si and Fe multilayers [12,15], the present results indicate that the paramagnetic silicide sublayer in the Si/Fe interfaces is identical in both Si-on-Fe and Fe-on-Si interfaces, while an asymmetry is revealed in the composition of the magnetic silicide sublayer. The main experimental difference with respect to those previous works is that the Fe and Si layer thickness is larger in the present samples. This has allowed us to assert that each studied sample would provide information on a single Si/Fe interface, which was checked with the S-m sample.

In view of the composition depth profile of the interfaces a picture of the reactions during the deposition process emerges. When Fe is deposited on Si, the paramagnetic Si-rich FeSi-type phase is readily produced and a thin ferromagnetic $Fe_{1-x}Si_x$ alloy sublayer also develops. However, when Si is deposited on Fe, the $Fe_{1-x}Si_x$ is first formed as high Si concentration magnetic silicide and finally the paramagnetic c-$Fe_{1-x}Si$ is formed with the available Fe. In either case, the c-$Fe_{1-x}Si$ phase consists of only a few monolayers.

Acknowledgments

The financial support of the Spanish MINECO MAT2011-23791, the President of Russia Grant (NSh-1044.2012.2), RFFI Grant 13-02-01265, the Ministry of Education and Science of Russian Federation (14.604.21.0002 and 02G25.31.0043), Aragonese DGA-IMANA E34 (cofunded by Fondo Social Europeo) and that received from the European Union FEDER funds is acknowledged. L.B.R. acknowledges the Spanish MINECO FPU 2010 grant.

References

[1] M.N. Baibich, J.M. Broto, A. Fert, F.N. Van Dau, F. Petroff, P. Etienne, G. Creuzet, A. Friederich, J. Chazelas, Phys. Rev. Lett. 61 (1988) 2472–2475.
[2] R.E. Camley, R.L. Stamps, J. Phys.: Condens. Matter 5 (1993) 3727.
[3] G.S. Patrin, N.V. Volkov, V.P. Kononov, JETP Lett. 68 (1998) 307.
[4] G.S. Patrin, S.G. Ovchinnikov, D.A. Velikanov, V.P. Kononov, Phys. Solid State 43 (2001) 1712.
[5] G.S. Patrin, N.V. Volkov, S.G. Ovchinnikov, E.V. Eremin, M.A. Panova, S.N. Varnakov, JETP Lett. 80 (2004) 491.
[6] S. Datta, B. Das, Appl. Phys. Lett. 56 (1990) 655.
[7] G. Binasch, P. Grünberg, F. Saurenbach, W. Zinn, Phys. Rev. B 39 (1989) 4828–4830.
[8] S. Wolf, L. Jiwei, M.R. Stan, E. Chen, D.M. Treger, Proc. IEEE 98 (2010) 2155–2168.
[9] G.J. Strijkers, J.T. Kohlhepp, H.J.M. Swagten, W.J.M. de Jonge, Phys. Rev. Lett. 84 (2000) 1812–1815.
[10] R.R. Gareev, D.E. Bürgler, M. Buchmeier, D. Olligs, R. Schreiber, P. Grünberg, Phys. Rev. Lett. 87 (2001) 157202.
[11] R. Kläsges, C. Carbone, W. Eberhardt, C. Pampuch, O. Rader, T. Kachel, W. Gudat, Phys. Rev. B 56 (1997) 10801–10804.
[12] G.J. Strijkers, J.T. Kohlhepp, H.J.M. Swagten, W.J.M. de Jonge, Phys. Rev. B 60 (1999) 9583–9587.
[13] S.R. Naik, S. Rai, G.S. Lodha, R. Brajpuriya, J. Appl. Phys. 100 (1) (2006) 013514.
[14] S.R. Naik, S. Rai, M.K. Tiwari, G.S. Lodha, J. Phys. D: Appl. Phys. 41 (11) (2008) 115307.
[15] A. Gupta, D. Kumar, V. Phatak, Phys. Rev. B 81 (2010) 155402.
[16] K. Konuma, J. Vrijmoeth, P.M. Zagwijn, J.W.M. Frenken, E. Vlieg, J.F. van der Veen, J. Appl. Phys. 73 (1993) 1104–1109.
[17] E. Chubunova, I. Khabelashvili, Y. Lebedinskii, V. Nevolin, A. Zenkevich, Thin Solid Films 247 (1) (1994) 39–43.
[18] E.E. Fullerton, J.E. Mattson, S.R. Lee, C.H. Sowers, Y.Y. Huang, G. Felcher, S.D. Bader, F.T. Parker, J. Appl. Phys. 73 (1992) 6335–6337.
[19] S. Degroote, M.H. Langelaar, T. Kobayashi, J. Dekoster, J.D. Watchter, R. Moons, L. Niesen, G. Langouche, Mater. Res. Soc. Symp. Proc. 320 (1994) 133.
[20] G. Crecelius, Appl. Surf. Sci. 65 (0) (1993) 683–689.
[21] J.M. Gallego, J.M. García, J. Alvarez, R. Miranda, Phys. Rev. B 46 (1992) 13339–13344.
[22] M.S. Platunov, S.N. Varnakov, S.M. Zharkov, G.V. Bondarenko, E. Weschke, E. Schierle, S.G. Ovchinnikov, JETP Lett. 99 (2014) 706.
[23] S.M. Amir, M. Gupta, A. Gupta, K. Ambika, J. Stahn, Appl. Surf. Sci. 277 (2013) 182–185.
[24] L. Badía-Romano, J. Rubín, C. Magén, D.E. Bürgler, J. Bartolomé, J. Appl. Phys. 116 (2) (2014) 023907.
[25] S.N. Varnakov, A.S. Parshin, S.G. Ovchinnikov, D. Rafaja, L. Kalvoda, A.D. Balaev, S.V. Komogortsev, Tech. Phys. Lett. 31 (2005) 947–950.
[26] A. Ishizaka, Y. Shiraki, J. Electrochem. Soc. 133 (1986) 666–671.
[27] L. Badía-Romano, J. Rubín, F. Bartolomé, J. Bartolomé, S. Ovchinnikov, S. Varnakov, C. Magén, J. Rubio-Zuazo, G.R. Castro, Spin 4 (2014) 1–7.
[28] D.R. Lide, Handbook of Chemistry and Physics, CRC Press, Florida, 2004.
[29] L. Vocadlo, G. Price, I. Wood, Acta Crystallogr. Sect. B 56 (2000) 369.
[30] M. Fanciulli, G. Weyer, H. Känel, N. Onda, Phys. Scripta T54 (1994) 16.
[31] K.L. Whiteaker, I.K. Robinson, C. Benson, D.M. Smilgies, N. Onda, H. von Känel, Phys. Rev. B 51 (1995) 9715–9721.
[32] D. Briggs, J.T. Grant, Surface Analysis by Auger and X-ray Photoelectron Spectroscopy, IM Publications and Surface Spectra Limited, Chichester, 2003.
[33] F.J. Himpsel, F.R. McFeely, A. Taleb-Ibrahimi, J.A. Yarmoff, G. Hollinger, Phys. Rev. B 38 (1988) 6084–6096.
[34] B. Egert, G. Panzner, Phys. Rev. B 29 (1984) 2091–2101.
[35] T. Cottineau, M. Morin, D. Bélanger, ECS Trans. 19 (35) (2009) 1.
[36] A. Gheorghiu, G. Dufour, F. Ténégal, C. Sénémaud, Nanostructured Silicon-based Powders and Composites, Taylor and Francis, London, 2003.
[37] A. Jablonski, C.J. Powell, J. Vac. Sci. Technol. A 21 (1) (2003) 274.
[38] A. Jablonski, C.J. Powell, J. Vac. Sci. Technol. A 27 (2) (2009) 253.
[39] C.J. Powell, A. Jablonski, NIST Standard Reference Data Program Database (SDR 71), NIST Electron Inelastic-mean-free-path Database, Version 1.1, US Department of Commerce, National Institute of Standards and Technology, Gaithersburg, MD, 2000.
[40] A. Jablonski, F. Salvat, C.J. Powell, NIST Elastic-Scattering Cross-Section Database (SDR 64), NIST Electron Elastic-scattering cross-section Database, Version 3.1, US Department of Commerce, National Institute of Standards and Technology, Gaithersburg, MD, 2003.
[41] I.N. Shabanova, V.A. Trapeznikov, J. Electron Spectrosc. Relat. Phenom. 6 (1975) 297.
[42] V. Kinsinger, I. Dezsi, P. Steiner, G. Langouche, J. Phys.: Condens. Matter 2 (22) (1990) 4955.
[43] S. Hong, P. Wetzel, G. Gewinner, D. Bolmont, C. Pirri, J. Appl. Phys. 78 (9) (1995) 5404–5411.
[44] B. Li, M. Ji, J. Wu, C. Hsu, J. Appl. Phys. 68 (3) (1990) 1099.